SERCA2a-activating PLB mutant improves calcium handling in dilated cardiomyopathy model of hiPSC-CMs.

Daniel R. Stroik[1], Delaine K. Ceholski[2], Paul F. Thanel[1], Philip A. Bidwell[1], Joseph M. Autry[1], Razvan L. Cornea[1], David D. Thomas[1,3]

[1]Department of Biochemistry, Molecular Biology, and Biophysics, University of Minnesota, Minneapolis, Minnesota 55455
[2]Cardiovascular Research Center, Icahn School of Medicine at Mount Sinai, New York City, New York 10029

[3]To whom correspondence may be addressed:
[3]David D. Thomas, University of Minnesota, Dept. of Biochemistry, Molecular Biology, and Biophysics, 6-155 Jackson Hall, 321 Church St. S.E., Minneapolis, MN 55455, USA. Email: ddt@umn.edu; Tel: +1 (612) 625-0957

Abstract

There is increasing momentum toward the development of gene therapy for heart failure, cardiomyopathy, and chronic cardiac diseases attributed to impaired calcium (Ca) transport and reduced contractility. Here, we established a novel FRET assay using fluorescently-tagged SERCA2a (the cardiac Ca pump) and PLB (its endogenous regulator) that directly tests the capacity of loss-of-function PLB mutants (PLB_M) to compete with wild-type PLB (PLB_{WT}) to relieve SERCA2a inhibition. The combination of a mutation conferring loss-of-inhibitory-function (L31A-PLB_M) and a mutation associated with increased binding affinity (I40A-PLB_M) resulted in a PLB_M (L31A/I40A) capable of displacing PLB_{WT}. Overexpression of L31A/I40A-PLB_M increased Ca-ATPase activity in PLB_{WT}-expressing HEK293-6E cells. In human induced pluripotent stem cell derived cardiomyocytes (hiPSC-CMs) from healthy individuals, recombinant adeno-associated virus 2 (rAAV2) driven expression of L31A/I40A-PLB_M significantly enhanced Ca-release amplitude and removal. Furthermore, L31A/I40A-PLB_M expression in a hiPSC-CM dilated cardiomyopathy fully rescued irregular Ca transients and decreased Ca transport. Taken together, these results suggest that gene transfer of PLB_M is a potential therapy for cardiac diseases associated with impaired Ca transport and muscle contractility.

1. Introduction

Heart failure (HF) is a cardiac pathology characterized by the impaired capacity of the ventricle to fill with or eject blood, and constitutes one of the leading causes of morbidity and mortality worldwide.[1] Over the last decade, researchers have made significant progress in understanding the intracellular and molecular mechanisms that are altered during HF progression. Defects in sarcoplasmic reticulum (SR) Ca transport has been identified as a potential determinant of decreased contractility in the failing hearts.[2-4] Ca transport from the cytosol to the SR lumen in cardiomyocytes (CM) is largely executed (~70% of Ca molecules transported) via the SR Ca-ATPase (SERCA2a).[5] Despite recent advances in device and pharmacological therapies, rates of heart disease continue to rise due to an aging population; thus, new treatment options are urgently needed. Our increasing knowledge of the molecular mechanisms fundamental to cardiac disease – including HF – has expanded the therapeutic potential to target key molecules involved in Ca handling including SERCA2a.

The activity of SERCA2a is regulated by phospholamban (PLB), a 52-residue, single-pass transmembrane protein expressed in the SR of cardiac muscle that binds to SERCA2a and reduces its apparent Ca affinity.[6] PLB is in equilibrium between homopentamers and monomers, where the oligomeric state is proposed to function as a reservoir.[7] Previous studies have identified two functional domains on transmembrane helix of PLB.[8-10] Mutations in one domain diminishes inhibitory function and with no effects on the oligomeric state(s), while mutations in the other domain increases binding between PLB and SERCA and shifts the equilibrium towards the monomeric state.

The regulation of gene expression has been investigated in healthy individuals and HF patients, and decreased SERCA-to-PLB ratio is associated with deteriorated cardiac function, indicating that SERCA/PLB stoichiometry and SERCA2a activity are potential therapeutic targets.[11-13] To this end, SERCA2a overexpression via recombinant adeno-associated virus (rAAV) was achieved in HF animal models to increase the SERCA-to-PLB ratio in the heart. SERCA2a overexpression was tolerated and significantly enhanced cardiac function in disease models by multiple metrics.[14,15] Recently, gene therapy designed to overexpress

SERCA2a in the heart underwent clinical trials in patients diagnosed with end-stage HF.[16] Despite positive preliminary results in Phase 1/2a,[17] the trial did not meet its primary end goals in phase 2b and this has been ascribed to dosage constraints.[18] One factor may be the large size of SERCA2a, which limits steady-state expression levels of the gene therapy construct. Other attempts to increase the SERCA-to-PLB ratio include expression of miRNAs that directly target PLB expression[19-21] and oligonucleotide-based drugs[22,23], although these strategies have not yet produced a viable drug.

In this study, we have pursued an alternative approach to activate SERCA2a by expressing a loss-of-function (LOF) PLB mutant (PLB_M) that competes with the inhibitory wild-type PLB (PLB_{WT}) (Figure 1A) via viral delivery. In this approach the ratio between endogenous SERCA and PLB is not altered, rather the endogenous inhibitory PLB_{WT} is displaced to enhance SERCA2a function. Thus, this strategy is designed to overcome limitations associated with SERCA2a overexpression-based gene therapy. FRET-based assays demonstrate that the combination of two PLB mutations: L31A-PLB_M (LOF) and I40A-PLB_M (associated with increased SERCA binding), result in a PLB_M (L31A/I40A) capable of displacing PLB_{WT}. In HEK293-6E cells expressing PLB_{WT}, overexpression of the L31A/I40A-PLB_M construct increased Ca-ATPase activity. We directly measured the effect of virally-delivered L31A/I40A-PLB_M on SR Ca transport in human induced pluripotent stem cell derived CMs (hiPSC-CMs) from healthy individuals and found that the AAV.PLB_M construct significantly enhanced Ca-release amplitude and removal compared to control cells. In a hereditary dilated cardiomyopathy model in hiPSC-CMs (R14del-PLB), AAV2.L31A/I40A-PLB_M corrects irregular Ca transients and improves Ca transport. These results suggest that gene transfer of PLB_M is viable therapy for cardiac diseases associated with impaired Ca transport and muscle contractility.

2. Methods

2.1 Molecular Biology

eGFP and tagRFP were fused to the N-terminus of human SERCA2a and human PLB, respectively. We have demonstrated that attachment of the fluorescent proteins at these sites does not interfere with the activity of SERCA nor inhibition by PLB.[24,25] PLB mutations were introduced using the QuikChange mutagenesis kit (Agilent Technologies, Santa Clara, CA), and all expression plasmids were sequenced for confirmation.

2.2 Cell Culture

Human embryonic kidney cells 293 (HEK293-6E, NRC, Canada) were cultured in FreeStyle F17 expression medium (Thermo Fisher Scientific, Waltham, MA) supplemented with 2 mM L-glutamine (Invitrogen, Waltham, MA). Cell cultures were maintained in shaker set at 125 rpm in an incubator at 37°C with 5% CO_2 (Forma Series II Water Jacket CO_2 Incubator, Thermo Fisher Scientific, Waltham, MA). For displacement assays, HEK293-6E cells were transiently transfected using 293fectamine with GFP-SERCA2a, RFP-PLB_{WT}, and PLB_M or empty vector in a 1:7:7 molar ratio. Cells were then assayed 48 hours post-transfection.

The control hiPSC line (SKiPS-31.3) was cultured as previously described.[26] The R14del hiPSC line was derived from the KSiPS-31.3 line using homologous recombination via CRISPR/Cas9. Monolayer cardiac differentiation was performed as described, yielding beating cardiomyocytes within 7-10 days.

2.3 Immunoblot

Samples were separated on a 4-20% polyacrylamide gradient gel (Bio-Rad, Hercules, CA) and transferred to polyvinylidene difluoride (PVDF) membrane. The PVDF membrane was blocked in Odyssey Blocking Buffer (LI-COR Biosciences, Lincoln, NE) followed by overnight incubation at 4 °C with the primary target antibody: rabbit anti-GFP polyclonal antibody (pAb) (1:1000; ab290, Abcam, Cambridge, United Kingdom), mouse anti-SERCA2 monoclonal antibody (mAb) (1:1000; 2A7-A1, Abcam), rabbit anti-tagRFP pAb (1:1000; ab233, Evrogen), mouse anti-PLB mAb (1:1000, 2D12, Abcam) or rabbit anti-β-actin pAb (1:5000, ab8227, Abcam). Blots were incubated with anti-mouse or anti-rabbit secondary antibodies conjugated to IRDye 680RD or IRDye 800CW, respectively, for 1 h at 23 °C (1:20,000; LI-COR Biosciences). Blots were quantified on the Odyssey scanner (LI-COR Biosciences).

2.4 Fluorescence Data Acquisition and Analysis

Fluorescence lifetime (FLT) measurements were conducted in a top-read FLT plate reader designed and built by Fluorescence Innovations, Inc. (St. Paul, MN) in 384-well plate formats. GFP donor fluorescence was excited with a 473 nm microchip laser from Concepts Research Corporation (Belgium, WI), and emission was acquired with 490 nm long-pass and 520/17 nm band-pass filters (Semrock, Rochester, NY). We previously demonstrated the performance of this plate reader with known fluorescence standards, as well as with a FRET-based HTS method that targets SERCA.[27,28] TRF waveforms from donor and FRET-labeled samples were analyzed as described in our previous publications and the supplemental methods.

2.5 Ca-ATPase Activity

An enzyme-coupled, NADH-linked ATPase assay was used to measure SERCA ATPase activity in 96-well microplates. Each well contained HEK293-6E homogenates, 50 mM MOPS (pH 7.0), 100 mM KCl, 1 mM EGTA, 0.2 mM NADH, 1 mM phosphoenol pyruvate, 10 IU/mL of pyruvate kinase, 10 IU/mL of lactate dehydrogenase, 3.5 µg/mL of the Ca ionophore A23187, and $CaCl_2$ added to set ionized $[Ca]_i$ to the desired values. The assay was started by addition of Mg-ATP at a final concentration of 5 mM and read in a SpectraMax 384 Plus microplate spectrophotometer from Molecular Devices (Sunnyvale, CA). The Ca-ATPase assays were conducted over a range of $[Ca]_i$, and the ATPase activities were fitted using the Hill function

$$V = \frac{V_{max}}{1 + 10 - \left(n(pK_{ca} - pCa)\right)} \qquad \textbf{Eq. (1)}$$

where V is the initial rate of Ca-dependent ATPase activity, V_{max} is the rate of Ca-ATPase activity at saturating $[Ca]_i$, n is the Hill coefficient, and pK_{Ca} is the apparent Ca dissociation constant.

2.6 Ca transient measurements

hiPSC-CMs (day 25 of differentiation) were enzymatically dissociated using the Detach 2 kit (Promocell, Heidelberg, Germany) and plated on Matrigel-coated German glass coverslips. After 2 days, the plated hiPSC-CMs were loaded with a Ca-sensitive fluorescent dye (Fura-2 AM, cell permeant, ThermoFisher, Rockville, MD, USA) and the ratios of fluorescence intensities (excitation ratio of 340/380 nm) were recorded using the IonOptix system (Ionoptix, Milton, MA). The electrically-induced Ca transients were triggered by pulses from a MyoPacer (IonOptix, Milton, MA) at 40V and 0.5 Hz and measurements were obtained at room temperature. Ca traces were analyzed using IonWizard software (IonOptix) to calculate the amplitude (peak height relative to baseline), and tau (time of relaxation). Number of irregular Ca transients was quantified using IonOptix software.

For the AAV2.L31A/I40A PLB virus, hiPSC-CMs were infected at day 20 of differentiation (1e4 MOI), enzymatically dissociated on day 23, and plated on Matri-gel coated German glass coverslips, as described above. Measurements were made at day 25 and compared to non-infected control hiPSC-CMs. Virus was purified according to the two-plasmid method with iodixanol gradient as described.

2.7 Gene expression

RNA was extracted from uninfected and AAV-infected hiPSC-CMs at day 25, and cDNA was synthesized as previously described. Gene expression compared to the housekeeping gene β2-microglobulin was determined using qRT-PCR, as assessed by $\Delta\Delta C_t$ analysis. See Supplemental Table 1 for the list of primers.

2.8 Statistical analysis

All statistics were performed using Prism (GraphPad, La Jolla, CA) and analysis was done by one-way ANOVA followed by the Bonferroni post hoc test; analysis of two group comparisons was done by Student's t-test (*P < 0.05, **P < 0.01, ***P < 0.001, $^{\#}$P < 0.0001, and 'ns' is not significant). Data is presented as mean ± standard error of the mean (SEM), and all values were obtained from a minimum of three separate experiments.

3. Results

3.1 FRET measurement of competition between PLB_{WT} and loss-of-function PLB_M

Previously, two classes of point mutations within the PLB transmembrane domain have been identified (via alanine-scanning mutagenesis) with disparate functional outcomes: loss-of-inhibitory function (LOF) and gain-of-binding affinity (GOB) mutations.[8] We hypothesized that the combination of these mutation types in a single PLB peptide would result in LOF-PLB that can effectively compete with the inhibitory PLB_{WT}. To test this, we developed a SERCA2a-PLB biosensor system by expressing GFP-tagged SERCA2a and RFP-tagged PLB_{WT} in HEK293-6E cells and measuring time-resolved FRET as a readout for changes in SERCA2a-PLB complex structure and binding. We varied the ratio between the donor molecule (GFP-SERCA2a) and acceptor molecule (RFP-PLB_{WT}), and found that the maximal energy transfer efficiency E (fractional decrease of the fluorescence lifetime) in this live cell based system saturates at a 0.10, as previously reported.[27] We transfected cells expressing GFP-SERCA2a and RFP-PLB_{WT} with either untagged PLB_{WT} or PLB_M containing transmembrane mutations (L31A, I40A, or L31A/I40A). Displacement of the RFP-PLB_{WT} was measured as a decrease in the FRET efficiency normalized to the GFP-SERCA/RFP-PLB_{WT} only cells (Figure 1B). FRET between GFP-SERCA2a and RFP-PLB_{WT} decreased significantly upon addition of unlabeled PLB_{WT}, indicating that the RFP-PLB_{WT} and unlabeled PLB_{WT} are in equilibrium for hetero-dimeric binding to GFP-SERCA2a. An alanine substitution at leucine 31 (L31A; LOF mutation) did not alter the FRET value relative to the wild-type control. In contrast, an alanine substitution at isoleucine 40 (I40A; associated with increased SERCA binding) further decreased the FRET value, indicating that I40A-PLB_M competes effectively with RFP-PLB_{WT} with a potency (affinity) equal to or greater than that unlabeled PLB_{WT}. The combination of L31A/I40A mutations resulted in PLB_M with potency equal to that of I40A-PLB_M, supporting our hypothesis that PLB_M with both mutation types retains high affinity towards SERCA2a.

Expression of the constructs was confirmed by SDS-PAGE and immunoblot in boiled samples, which disrupts PLB pentamers, and in heated samples, which maintains the pentameric PLB state (Figure 1C and D). GFP-tagged SERCA2a was resolved from endogenous SERCA2b, as verified by binding of a GFP-specific antibody. There no bands of lower mobility and no apparent aggregation in intact cells. Expression of RFP-PLB produced a single band recognized by RFP- and PLB-specific antibodies. The presence of the I40A mutation disrupts pentamer formation and we observed the disappearance of the band corresponding to PLB_M pentamer when the I40A mutation is present (Figure 1D; lanes 11 and 12). PLB pentamer was detected in PLB_{WT} and L31A-PLB (Figure 1D; lanes 13 and14). As the expression of GFP-SERCA2a, RFP-PLB_{WT}, and PLB_M is not significantly different between respective samples, the observed changes in FRET is likely due to displacement of the wild-type RFP-tagged PLB via competitive binding (to GFP-SERCA2a) by the untagged PLB_M. The Ca-ATPase function of N-terminally tagged SERCA is identical to untagged SERCA, thus the tag does not disrupt the endogenous function.[25]

3.2 Effects of loss-of-function PLB mutations on the apparent Ca-affinity of SERCA2a

The effects of PLB_M expression on the apparent Ca-affinity of SERCA2a were determined in HEK293-6E homogenate samples, enabling co-expression of PLB_{WT} and PLB_M in a cell-based system similar to the FRET assays. Ca-ATPase activity in HEK293-6E cells overexpressing SERCA2a alone (Figure 2A, black) increases with Ca at physiological Ca concentrations (*e.g.,* between pCa 7 and pCa 6) and saturates at higher Ca concentrations (pCa 5), consistent with previous measurements. Concomitant expression of SERCA2a and inhibitory PLB_{WT} (Figure 2A and B, dark gray) decreases the apparent Ca-affinity, and the additional expression of PLB_{WT} (light blue) or L31A-PLB_M (light gray) does not further decrease the apparent Ca-affinity; indicating that SERCA2a is fully inhibited and that L31A-PLB_M does not relieve PLB_{WT} inhibition. We observed a further decrease in the apparent Ca-affinity upon co-expression of SERCA2a, PLB_{WT}, and I40A-PLB_M (red), suggesting that I40A-PLB_M preferentially binds to SERCA2a (consistent with FRET measurements) and acts as a super-inhibitor. Co-expression with L31A/I40A-PLB_M (green) increased Ca affinity to values similar to the SERCA-only sample, indicating that the PLB inhibition is relieved. Taken together, the structural (FRET) and functional (Ca-ATPase) results suggest that the L31A/I40A-PLB_M is non-inhibitory and binds to SERCA2a.

3.3 rAAV-driven expression of L31A/I40A mutant enhances Ca transient parameters in hiPSC-CMs

Given the promising results using the L31A/I40A-PLB_M in FRET and Ca-ATPase assays in HEK293-6E cells, we tested the effects of AAV-delivered PLB_M in human cardiomyocyte models. We infected hiPSC-CMs with AAV2.L31A-, AAV2.I40A-, or AAV2.L31A/I40A-PLB_M at day 20 and recorded Ca transients at day 25 (Figure 3A). We observed a striking improvement in Ca transient parameters (peak amplitude, removal rate, rythmogenicity) of hiPSC-CMs upon infection with AAV2.L31A/I40A-PLB_M, but not with AAV2.L31A-PLB_M or AAV2.I40A-PLB_M (Figure 3B and C). This suggests that activation of Ca-transport also increases the Ca SR-load and the Ca released (upon electrical stimulation). We observed no differences in SERCA2a or cardiac

Troponin T expression levels (Figure 3D); however, the total amount of PLB in the viral-infected hiPSC-CMs was approximately 3-fold higher than uninfected controls with the difference coming from exogenous virally-expressed PLB (Figure 3D).

3.4 SERCA2a activators rescue irregular Ca transients in the cardiomyopathy-causing R14del PLB hiPSC-CMs

Next, we sought to test whether rAAV2.L31A/I40A-PLB is capable of rescuing aberrant Ca handling in disease-relevant models. R14del-PLB causes dilated cardiomyopathy characterized by LV dilation, decreased ejection fraction, and, most notably, arrhythmia (tachycardia and fibrillation). Previous work in patient-derived R14del-PLB hiPSC-CMs showed irregular Ca transients after day 35 of differentiation and this was rescued by either gene correction by TALENs or infection of an AAV expression a miRNA to knockdown endogenous PLB and express codon-optimized wild-type PLB.[29] We genome engineered R14del-PLB hiPSCs using homologous recombination via CRISPR/Cas9 to insert the R14del-PLB mutation into the control SKiPS-31.3 line so that we have an isogenic control to test our therapies.

The R14del-PLB hiPSC-CMs show the characteristic irregular Ca transients observed after day 35 of differentiation at a frequency of 0.58 ± 0.19 (n=85). Upon infection with rAAV2.L31A/I40A-PLB we observed an improvement in Ca handling properties of the R14del-PLB hiPSC-CMs. Representative Ca tracings show a significant reduction in irregular Ca transients (Figure 4A) and both Ca amplitude and tau are improved with rAAV2.L31A/I40A-PLB infection (Figure 4B and C). Finally, no irregular Ca transients (n=20) were observed upon infection with rAAV2.L31A/I40A-PLB.

4. Brief Discussion

We demonstrated previously that the interaction between the cardiac Ca pump, SERCA2a, and its inhibitor, PLB, can be measured via FRET in HEK293 cell system.[27] In the present study, we establish a novel FRET assay to measure the competition of unlabeled, non-inhibitory PLB_M and RFP-labeled PLB_{WT} for binding to the GFP-SERCA2a. We used this assay to measure the relative affinity of non-inhibitory PLB_M and identified a double mutant (L31A/I40A) that binds with affinity greater than the wild-type PLB. We tested effects of the overexpression of L31A/I40A-PLB_M on Ca-ATPase activity and found that the construct increases Ca-transport in HEK293 cells. In hiPSC-CMs, we found that rAAV2-dependent expression of L31A/I40A-PLB_M significantly improved Ca-release amplitude and removal in both healthy and pathogenic cell lines. This work suggests that gene transfer of non-inhibitory L31A/I40A-PLB_M is a potential therapeutic for heart diseases caused by impaired Ca transport and decreased muscle contractility.

Acknowledgments

We thank Bengt Svensson for help with figures. Spectrophotometric assays were performed in the Biophysical Technology Center at the University of Minnesota Department of Biochemistry, Molecular Biology, and Biophysics. This study was supported in part by National Institutes of Health grants to D.D.T. (R01 GM27906, R01 HL129814, and R37 AG26160).

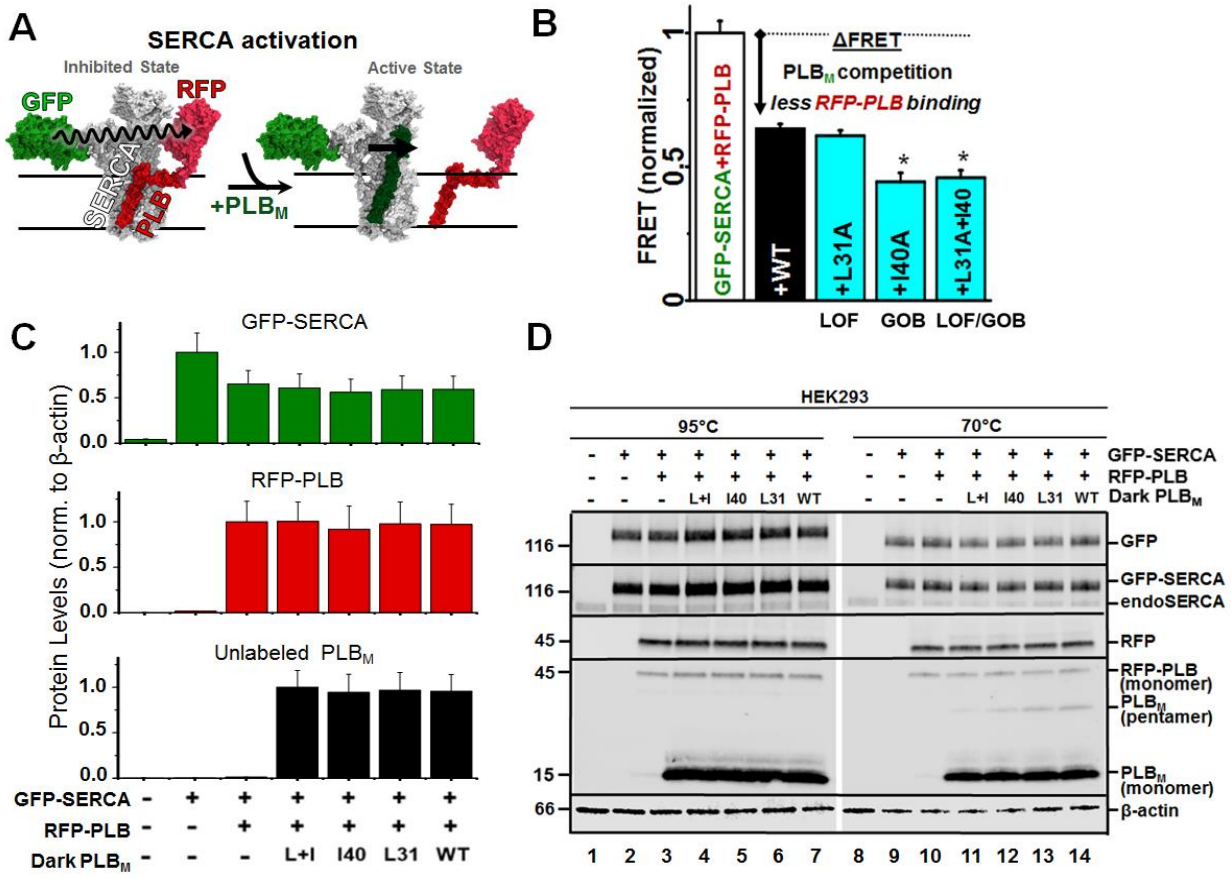

Figure 1. SERCA activation by PLB_M competition. *A:* PLB mutant (PLB_M, dark green) displaces inhibitory RFP-PLB (PLB_{WT}, dark red) resulting in a FRET decrease. *B:* FRET assay of PLB_M competition in HEK293-6E. GFP-SERCA-RFP-PLB_{WT} FRET (binding, *white bar*) is decreased (arrow) by PLB variants. LOF = Loss-of-inhibitory function mutation. GOB = Gain-of-binding mutation. *C/D:* Immunoblots of homogenates boiled at 95°C (lanes 1-7) or heated at 70°C (lanes 8-14) from untransfected HEK293-6E cells (lane 1&8), cells expressing GFP-SERCA2a (lanes 2&9), or cells expressing GFP-SERCA2a+RFP-PLB (lanes 3-7&11-14) +L31A/I40A-PLB (lanes 4&11), +I40A-PLB (lanes 5&12), +L31A-PLB (lanes 6&13), and +WT-PLB (lanes 7&14). Antibodies from top to bottom are anti-GFP, anti-SERCA2, anti-RFP, anti-PLB, and anti-β-actin. Quantification of steady-state expression levels by densitometry for boiled samples (lanes 1-7). Error bars indicate SEM (n=3). *P < 0.05.

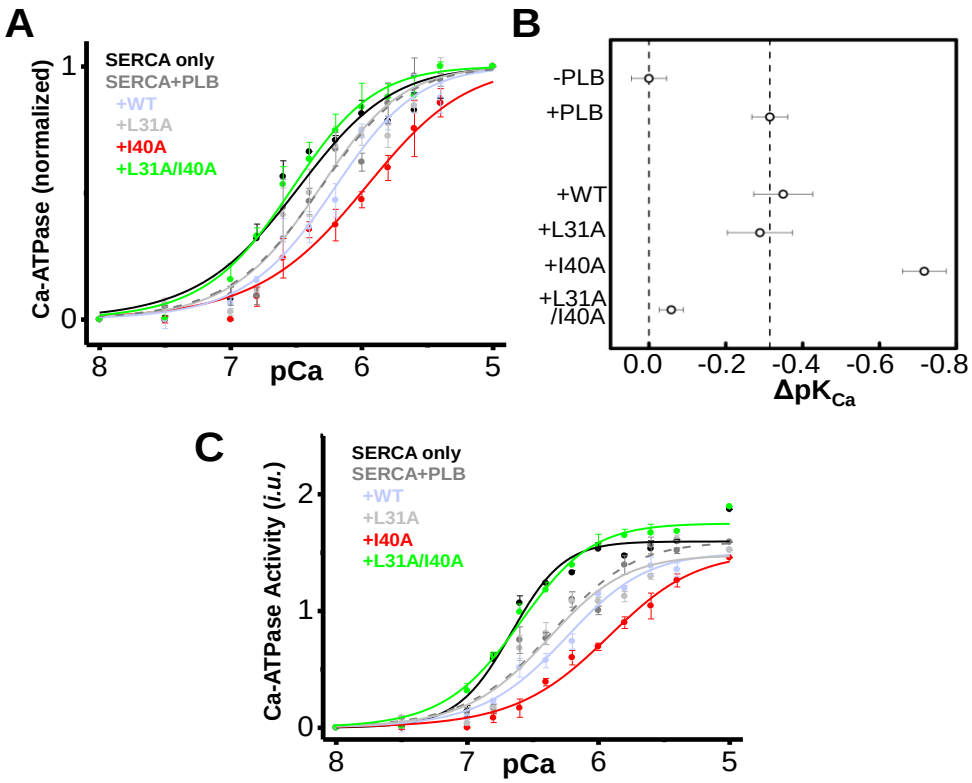

Figure 2. Ca-ATPase assays measuring effects of PLB_M on SERCA-dependent Ca transport. *A:* Normalized Ca-ATPase activity of HEK293-6E cells was measured 48 hours after transfection using +empty vector (negative control, not shown), +WT-SERCA2a (black), +WT-SERCA2a/WT-PLB (dark gray, dotted line), +WT-SERCA2a/WT-PLB +WT-PLB (blue), +WT-SERCA2a/WT-PLB +L31A-PLB (light grey), WT-SERCA2a/WT-PLB +I40A-PLB (red), or WT-SERCA2a/WT-PLB +L31A/I40A-PLB (green). *B:* Quantification of *apparent* Ca affinity (pK_{Ca}) from *A*. *C:* Non-normalized Ca-ATPase activity from *A*. Error bars indicate SEM (n=3). *P < 0.05.

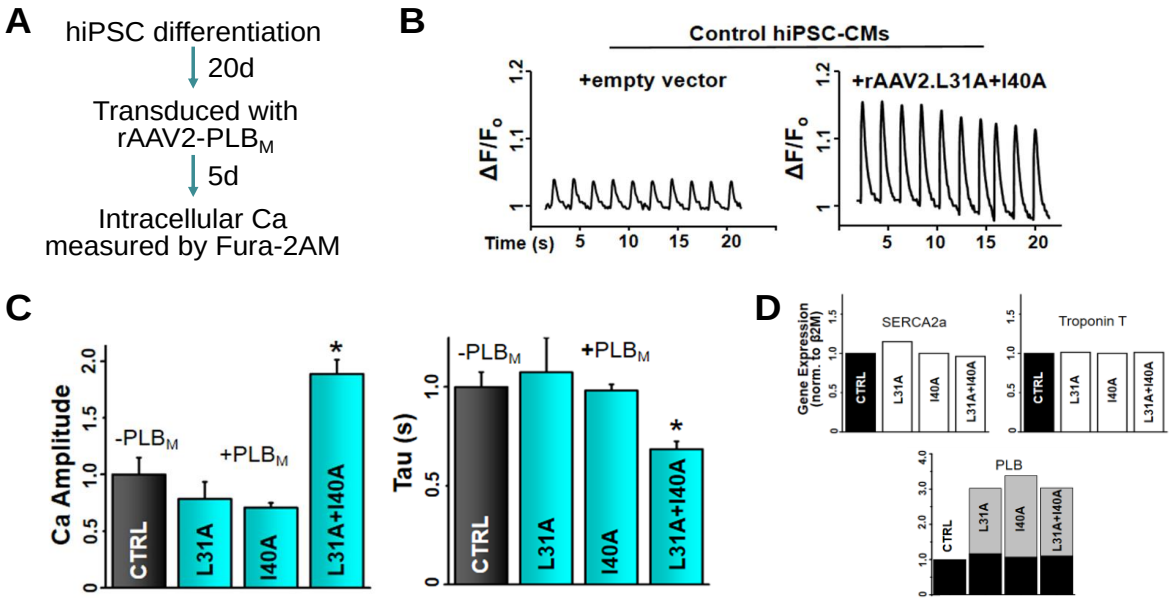

Figure 3. In normal, healthy hiPSC-CMs, rAAV2-driven expression of L31A/I40A-PLB significantly enhances Ca-release amplitude and removal. *A:* Schematic of experimental design for hiPSC differentiation. *B:* qRT-PCR analysis of gene expression of Ca transport and contractility proteins: SERCA2a *(left)*, cardiac troponin T *(center)*, and PLB *(right;* black = endogenous PLB_{WT}, gray = exogenous PLB_M*)* of uninfected (CtRL) or infected (rAAV2-L31A/I40A PLB) hiPSC-CMs. All gene expression values are normalized to uninfected control. *C:* Representative trace of Ca transients in control hiPSC-CMs *(left)* compared to rAAV2-L31A/I40A PLB transduced hiPSC-CMs *(right)*. *D:* Quantification of Ca amplitude (peak height as a percentage of the baseline) normalized to uninfected control (CTRL) and time for relaxation (tau; seconds) of hiPSC-CMs normalized to uninfected control (CTRL). Error bars indicate SEM (n=3). *P < 0.05.

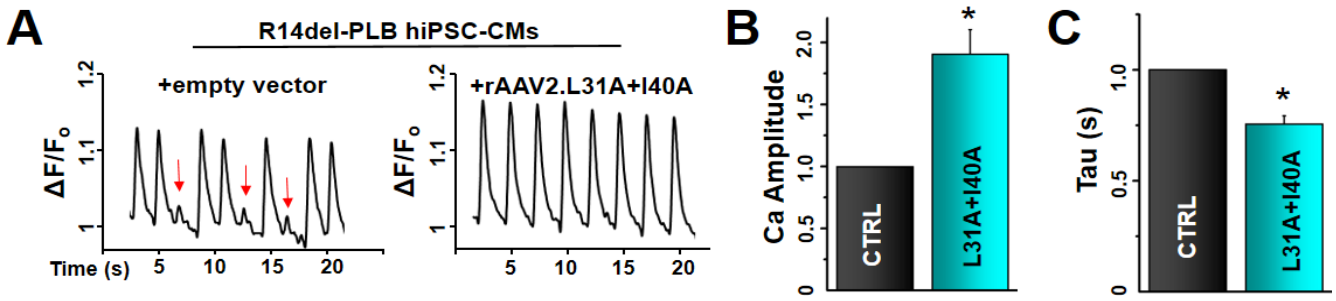

Figure 4. In R14del hiPSC-CMs, viral delivery of L31A/I40A-PLB rescues arrhythmogenic Ca transients. *A:* Representative traces of Ca transients in R14del PLB hiPSC-CMs (left) compared to R14del hiPSC-CMs infected with rAAV2.L31A/I40A-PLB (right). Irregular Ca transients highlighted by red arrow. *B:* Ca amplitude (peak height as a percentage of the baseline) normalized to uninfected R14del hiPSC-CMs. *C:* Time for relaxation (tau; seconds) normalized to uninfected R14del hiPSC-CMs. Error bars indicate SEM (n=3). *P < 0.05.

Supplementary Methods:

Fluorescence Data Acquisition and Analysis

The measured time-resolved fluorescence waveform,

$$I(t) = \int_{-\infty}^{\infty} IRF(t - t') \cdot F(t')dt' \quad \textbf{Eq. (2)}$$

is a function of the nanosecond decay time t, and is modeled as the convolution integral of the measured instrument response function, IRF(t), and the fluorescence decay model, *F*(t). The fluorescence decay model

$$F_{D+A}(t) = x_D F_D(t) + (1 - x_D)\, F_{DA}(t) \quad \textbf{Eq. (3)}$$

is a linear combination of a donor-only fluorescence decay function F_D(t) and an energy transfer-affected donor fluorescence decay F_{DA}(t). The donor decay F_D(t) is a sum of *n* exponentials

$$F_D(t) = \sum_{i=1}^{n} A_i\, exp(-t/\tau_i) \quad \textbf{Eq. (4)}$$

with discrete FLT species τ_i and pre-exponential mole fractions A_i. For the GFP donor, two exponentials (*n* = 2) were required to fit the observed fluorescence. The energy transfer-affected donor decay function, F_{DA}(t),

$$F_{DA}(t) = \sum_{j=1}^{N} X_j \cdot T_j(t) \quad \textbf{Eq. (5)}$$

is a sum over multiple structural states (*j*) with mole fractions X_j, represented by FRET-affected donor fluorescence decays T_j(t). The increase in the donor decay rate (inverse donor FLT) due to FRET is given by the Förster equation

$$k_{Ti} = k_{Di}(R/R_{0i})^{-6}, \text{ where} \quad \textbf{Eq. (6)}$$

$$k_{\mathrm{DAi}} = k_{\mathrm{Di}} + k_{\mathrm{Ti}}, \text{ and} \quad \textbf{Eq. (7)}$$

$$k_{Di} = 1/\tau_i \quad \textbf{Eq. (8)}$$

Supplementary Table 1. Primers used in qPCR.

Gene	Forward Primer (5`→3`)	Reverse Primer (5`→3`)
SERCA2a	CTGTCCATGTCACTCCACTTCC	AGCGGTTACTCCAGTATTGCAG
Cardiac TnT	AAGAGGCAGACTGAGCGGGAAA	AGATGCTCTGCCACAGCTCCTT
Endogenous PLB	ACAGCTGCCAAGGCTACCTA	GCTTTTGACGTGCTTGTTGA
Exogenous PLB (AAV-expressed)	TCAATTACGGGGTCATTAGTTC	ACTAATACGTAGATGTACTGCC
B2M	GGGATCGAGACATGTAAGCAG	CAAGCAAGCAGAATTTGGAA

Supplementary Figure 1.

1 Writing Group, M. *et al.* Heart Disease and Stroke Statistics-2016 Update: A Report From the American Heart Association. *Circulation* **133**, e38-360, doi:10.1161/CIR.0000000000000350 (2016).

2 Marks, A. R. Calcium cycling proteins and heart failure: mechanisms and therapeutics. *J Clin Invest* **123**, 46-52, doi:10.1172/JCI62834 (2013).

3 Ablorh, N. A. & Thomas, D. D. Phospholamban phosphorylation, mutation, and structural dynamics: a biophysical approach to understanding and treating cardiomyopathy. *Biophysical reviews* **7**, 63-76, doi:10.1007/s12551-014-0157-z (2015).

4 Gorski, P. A., Ceholski, D. K. & Hajjar, R. J. Altered myocardial calcium cycling and energetics in heart failure--a rational approach for disease treatment. *Cell Metab* **21**, 183-194, doi:10.1016/j.cmet.2015.01.005 (2015).

5 Bers, D. M. Calcium cycling and signaling in cardiac myocytes. *Annu Rev Physiol* **70**, 23-49, doi:10.1146/annurev.physiol.70.113006.100455 (2008).

6 MacLennan, D. H. & Kranias, E. G. Phospholamban: a crucial regulator of cardiac contractility. *Nat Rev Mol Cell Biol* **4**, 566-577, doi:10.1038/nrm1151 (2003).

7 Robia, S. L. *et al.* Forster transfer recovery reveals that phospholamban exchanges slowly from pentamers but rapidly from the SERCA regulatory complex. *Circ Res* **101**, 1123-1129 (2007).

8 Kimura, Y., Kurzydlowski, K., Tada, M. & MacLennan, D. H. Phospholamban inhibitory function is activated by depolymerization. *J Biol Chem* **272**, 15061-15064, doi:10.1074/jbc.272.24.15061 (1997).

9 Cornea, R. L., Jones, L. R., Autry, J. M. & Thomas, D. D. Mutation and phosphorylation change the oligomeric structure of phospholamban in lipid bilayers. *Biochemistry* **36**, 2960-2967, doi:10.1021/bi961955q (1997).

10 Simmerman, H. K., Kobayashi, Y. M., Autry, J. M. & Jones, L. R. A leucine zipper stabilizes the pentameric membrane domain of phospholamban and forms a coiled-coil pore structure. *J Biol Chem* **271**, 5941-5946, doi:10.1074/jbc.271.10.5941 (1996).

11 Hasenfuss, G. *et al.* Relation between myocardial function and expression of sarcoplasmic reticulum Ca(2+)-ATPase in failing and nonfailing human myocardium. *Circ Res* **75**, 434-442 (1994).

12 Mercadier, J. J. *et al.* Altered sarcoplasmic reticulum Ca2(+)-ATPase gene expression in the human ventricle during end-stage heart failure. *J Clin Invest* **85**, 305-309, doi:10.1172/JCI114429 (1990).

13 Nagai, R. *et al.* Regulation of myocardial Ca2+-ATPase and phospholamban mRNA expression in response to pressure overload and thyroid hormone. *Proc Natl Acad Sci U S A* **86**, 2966-2970, doi:10.1073/pnas.86.8.2966 (1989).

14 Schmidt, U. *et al.* Restoration of diastolic function in senescent rat hearts through adenoviral gene transfer of sarcoplasmic reticulum Ca(2+)-ATPase. *Circulation* **101**, 790-796 (2000).

15 Byrne, M. J. *et al.* Recirculating cardiac delivery of AAV2/1SERCA2a improves myocardial function in an experimental model of heart failure in large animals. *Gene Ther* **15**, 1550-1557, doi:10.1038/gt.2008.120 (2008).

16 Jessup, M. *et al.* Calcium Upregulation by Percutaneous Administration of Gene Therapy in Cardiac Disease (CUPID): a phase 2 trial of intracoronary gene therapy of sarcoplasmic reticulum Ca2+-ATPase in patients with advanced heart failure. *Circulation* **124**, 304-313, doi:10.1161/CIRCULATIONAHA.111.022889 (2011).

17 Zsebo, K. *et al.* Long-term effects of AAV1/SERCA2a gene transfer in patients with severe heart failure: analysis of recurrent cardiovascular events and mortality. *Circulation research* **114**, 101-108, doi:10.1161/CIRCRESAHA.113.302421 (2014).

18 Greenberg, B. *et al.* Prevalence of AAV1 neutralizing antibodies and consequences for a clinical trial of gene transfer for advanced heart failure. *Gene Ther* **23**, 313-319, doi:10.1038/gt.2015.109 (2016).

19 Andino, L. M. *et al.* AAV-mediated knockdown of phospholamban leads to improved contractility and calcium handling in cardiomyocytes. *J Gene Med* **10**, 132-142, doi:10.1002/jgm.1131 (2008).

20 Grobetal, T. *et al.* A novel artificial microRNA expressing AAV vector for phospholamban silencing in cardiomyocytes improves Ca2+ uptake into the sarcoplasmic reticulum. *PLoS One* **9**, e92188, doi:10.1371/journal.pone.0092188 (2014).

21 Bish, L. T. *et al.* Cardiac gene transfer of short hairpin RNA directed against phospholamban effectively knocks down gene expression but causes cellular toxicity in canines. *Hum Gene Ther* **22**, 969-977, doi:10.1089/hum.2011.035 (2011).

22 Soller, K. J. *et al.* Rheostatic Regulation of the SERCA/Phospholamban Membrane Protein Complex Using Non-Coding RNA and Single-Stranded DNA oligonucleotides. *Sci Rep* **5**, 13000, doi:10.1038/srep13000 (2015).

23 Soller, K. J., Yang, J., Veglia, G. & Bowser, M. T. Reversal of Phospholamban Inhibition of the Sarco(endo)plasmic Reticulum Ca2+-ATPase (SERCA) Using Short, Protein-interacting RNAs and Oligonucleotide Analogs. *J Biol Chem* **291**, 21510-21518, doi:10.1074/jbc.M116.738807 (2016).

24 Gruber, S. J. *et al.* Discovery of enzyme modulators via high-throughput time-resolved FRET in living cells. *Journal of biomolecular screening* **19**, 215-222, doi:10.1177/1087057113510740 (2014).

25 Bidwell, P., Blackwell, D. J., Hou, Z., Zima, A. V. & Robia, S. L. Phospholamban binds with differential affinity to calcium pump conformers. *J Biol Chem* **286**, 35044-35050, doi:10.1074/jbc.M111.266759 (2011).

26 Ceholski, D. K. *et al.* Functional and transcriptomic insights into pathogenesis of R9C phospholamban mutation using human induced pluripotent stem cell-derived cardiomyocytes. *J Mol Cell Cardiol* **119**, 147-154, doi:10.1016/j.yjmcc.2018.05.007 (2018).

27 Stroik, D. R. *et al.* Targeting protein-protein interactions for therapeutic discovery via FRET-based high-throughput screening in living cells. *Sci Rep* **8**, 12560, doi:10.1038/s41598-018-29685-z (2018).

28 Schaaf, T. M. *et al.* High-Throughput Spectral and Lifetime-Based FRET Screening in Living Cells to Identify Small-Molecule Effectors of SERCA. *SLAS Discov* **22**, 262-273, doi:10.1177/1087057116680151 (2017).

29 Karakikes, I. *et al.* Correction of human phospholamban R14del mutation associated with cardiomyopathy using targeted nucleases and combination therapy. *Nat Commun* **6**, 6955, doi:10.1038/ncomms7955 (2015).